

Magnetic Phase Diagram of the $S=1/2$ Triangular-Lattice Heisenberg Antiferromagnet $\text{Ba}_3\text{CoNb}_2\text{O}_9$

Kazuya Yokota, Nobuyuki Kurita, and Hidekazu Tanaka

Department of Physics, Tokyo Institute of Technology,

Meguro-ku, Tokyo 152-8551, Japan

(Dated: June 24, 2014)

Abstract

We report the results of low-temperature thermal and magnetic measurements on $\text{Ba}_3\text{CoNb}_2\text{O}_9$ powder, described as a uniform triangular-lattice antiferromagnet (TLAF) with a fictitious spin- $1/2$. $\text{Ba}_3\text{CoNb}_2\text{O}_9$ is found to undergo two-step antiferromagnetic transitions at $T_{\text{N}1} = 1.39$ K and $T_{\text{N}2} = 1.13$ K. As the magnetic field is increased, both $T_{\text{N}1}$ and $T_{\text{N}2}$ monotonically decrease. The magnetic field vs temperature phase diagram indicates that the exchange interactions are nearly of the Heisenberg type with weak easy-axis anisotropy and that the exchange interaction between triangular lattices is crucial, in contrast to the case of the quasi-two-dimensional TLAF $\text{Ba}_3\text{CoSb}_2\text{O}_9$ [Susuki *et al.*, Phys. Rev. Lett. **110**, 267201 (2013)].

PACS numbers: 75.10.Jm, 75.40.Cx, 75.45.+j

I. INTRODUCTION

Triangular-lattice antiferromagnets (TLAFs) have long been a subject of active research in condensed matter physics [1–5]. For classical Heisenberg spins, the antiferromagnetic nearest-neighbor exchange interaction produces triangular spin ordering. However, the classical ground state cannot be determined uniquely in a magnetic field because the ground state is continuously degenerate. In the presence of quantum fluctuations, the classical degeneracy can be lifted, so that a specific ground state is stabilized by the so-called order-by-disorder mechanism [6]. A two-dimensional (2D) $S=1/2$ triangular-lattice Heisenberg antiferromagnet (TLHAF) is one of the simplest quantum frustrated systems. The combination of the reduced dimensionality, geometric frustration, and the smallest spin markedly enhances quantum fluctuations, which can trigger exotic quantum states. One macroscopic quantum manifestation predicted for 2D $S=1/2$ TLHAFs is the stabilization of the “up-up-down” spin structure under an applied field [7–12]. In the magnetization process, the quantum ground state appears as a magnetization plateau at one-third of the saturation magnetization M_s , whereas in the classical model, the magnetization increases monotonically with the magnetic field up to M_s .

In spite of intensive research on 2D $S=1/2$ TLHAFs, details of the quantum effects including the $1/3$ magnetization plateau have not been elucidated definitively. This is mostly due to the lack of a model material that satisfactorily realizes a 2D $S=1/2$ TLHAF. Thus far, most experimental studies on 2D $S=1/2$ TLHAFs in magnetic fields have focused on compounds comprising Cu^{2+} magnetic ions such as Cs_2CuX_4 ($X = \text{Cl}, \text{Br}$) [13, 14]. However, the arrangement of CuX_4 tetrahedra in Cs_2CuX_4 does not have trigonal symmetry, which leads to a spatially anisotropic triangular lattice. The low-symmetric crystal lattice produces an antisymmetric interaction of the Dzyaloshinskiy-Moriya (DM) type. For these reasons, the magnetic model of Cs_2CuX_4 becomes complicated.

Recently, we have shown that $\text{Ba}_3\text{CoSb}_2\text{O}_9$ closely approximates an ideal 2D $S=1/2$ TLHAF [15, 16]. In $\text{Ba}_3\text{CoSb}_2\text{O}_9$, magnetic Co^{2+} ions centered at CoO_6 octahedra form “uniform” triangular lattice layers as shown in Fig. 1(a). Owing to the octahedral crystal field and spin-orbit interaction, the effective spin of Co^{2+} can be represented by $S=1/2$ at low temperatures well below the spin-orbit coupling constant $\lambda/k_B \sim 250$ K [17–19]. Although crystal lattice of $\text{Ba}_3\text{CoSb}_2\text{O}_9$ is hexagonal, the crystal field is close to cubic field.

This leads to the almost isotropic g -factor and exchange interaction between effective spins, unlike those in typical Co^{2+} compounds [15, 16]. Actually, the electron paramagnetic resonance measurement revealed the almost isotropic g -factors of 3.84 and 3.87 for $H \parallel ab$ and $H \parallel c$, respectively [16].

When a magnetic field is applied parallel to the ab plane, the quantum $1/3$ magnetization plateau is clearly observed [16]. $\text{Ba}_3\text{CoSb}_2\text{O}_9$ is the first example for which it was experimentally shown that the entire magnetization process including the quantum $1/3$ plateau exhibits good quantitative agreement with theoretical calculations. In addition, we have found a possible high-field quantum state at approximately $3/5M_s$ for $H \parallel ab$. To obtain a deeper understanding of the quantum phenomena in TLHAFs, it is worth investigating similar Co^{2+} -based materials and to compare the similarities and differences between their magnetic properties.

In this paper, we thus study the Nb-analog compound, $\text{Ba}_3\text{CoNb}_2\text{O}_9$, through low-temperature magnetization and specific heat measurements. $\text{Ba}_3\text{CoNb}_2\text{O}_9$ crystallizes in a hexagonal structure with the space group $P\bar{3}m1$ [20–22]. Figures 1(b) and (c) show the crystal structure of $\text{Ba}_3\text{CoNb}_2\text{O}_9$. The crystal structure of $\text{Ba}_3\text{CoNb}_2\text{O}_9$ differs from that of $\text{Ba}_3\text{CoSb}_2\text{O}_9$ in the stacking pattern of nonmagnetic BO_6 ($B = \text{Nb}, \text{Sb}$) octahedra. Neighboring NbO_6 octahedra in $\text{Ba}_3\text{CoNb}_2\text{O}_9$ are linked sharing their corners, while for $\text{Ba}_3\text{CoSb}_2\text{O}_9$, neighboring SbO_6 octahedra are linked sharing their faces [20, 22, 23]. Because of the highly symmetric crystal structure, the antisymmetric DM interaction is absent between the first-, second- and third-neighbor spins in the triangular lattice and between all spin pairs along the c axis in both compounds.

II. EXPERIMENTAL DETAILS

$\text{Ba}_3\text{CoNb}_2\text{O}_9$ powder was prepared by the chemical reaction: $3\text{BaCO}_3 + \text{CoO} + \text{Nb}_2\text{O}_5 \rightarrow \text{Ba}_3\text{CoNb}_2\text{O}_9 + 3\text{CO}_2$. Reagent-grade materials were mixed in stoichiometric ratios and calcined at 1200°C for 20 h in air. $\text{Ba}_3\text{CoNb}_2\text{O}_9$ was sintered at 1500°C for more than 20 h after being pressed into a pellet. The brown powder samples obtained were confirmed to be $\text{Ba}_3\text{CoNb}_2\text{O}_9$ by X-ray diffraction.

The specific heat was measured in the temperature range of 0.5 K to 300 K and under magnetic fields of up to 9 T using a physical property measurement system (PPMS, Quantum

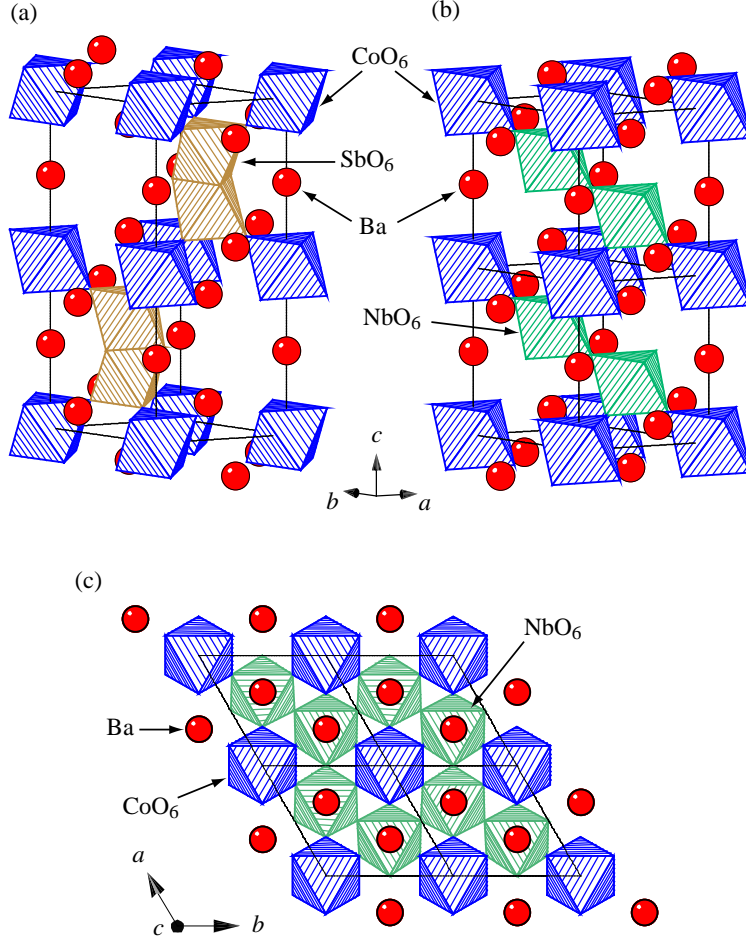


FIG. 1: (Color online) Schematic crystal structures of (a) $\text{Ba}_3\text{CoSb}_2\text{O}_9$ ($P6_3/mmc$) and (b) $\text{Ba}_3\text{CoNb}_2\text{O}_9$ ($P\bar{3}m1$). (c) Arrangement of CoO_6 and NbO_6 octahedra in $\text{Ba}_3\text{CoNb}_2\text{O}_9$ viewed along the c -axis. The solid lines show the chemical unit cell. For both compounds, magnetic Co^{2+} ions at the center of CoO_6 octahedra form a uniform triangular lattice in the ab plane.

Design) by the relaxation method. We also conducted magnetic measurements down to 0.4 K and up to 7 T using a SQUID magnetometer (MPMS XL, Quantum Design) equipped with an iHelium3 option (IQUANTUM).

III. RESULTS

The main panel of Fig. 2 shows the temperature dependence of the specific heat in $\text{Ba}_3\text{CoNb}_2\text{O}_9$ divided by the temperature C/T measured in the absence of a magnetic field. As the temperature decreases from 10 K, C/T increases gradually and exhibits two pro-

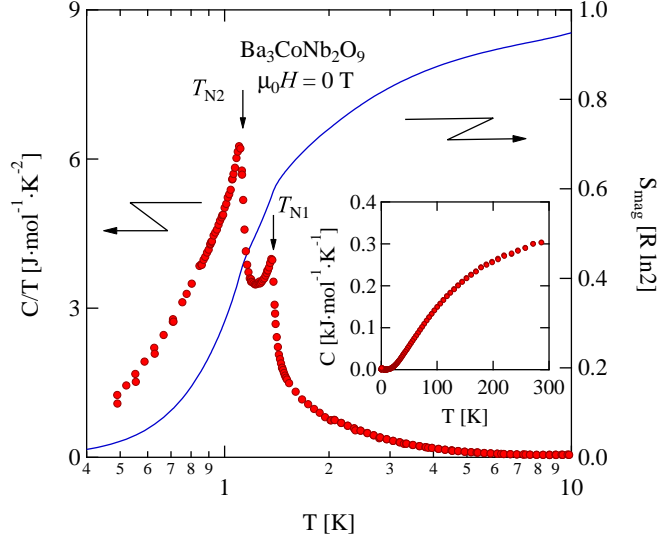


FIG. 2: (Color online) Temperature dependence of C/T in $\text{Ba}_3\text{CoNb}_2\text{O}_9$ measured at zero magnetic field. Magnetic phase transitions are observed at $T_{N1}=1.39$ K and $T_{N2}=1.13$ K, indicated by arrows. The solid curve represents the magnetic entropy S_{mag} in units of $R \ln 2$. The inset shows the specific heat below 300 K.

nounced peaks at $T_{N1}=1.39$ K and $T_{N2}=1.13$ K indicative of successive magnetic phase transitions. These two phase transitions are also confirmed by the magnetization measurements shown below.

Because $\text{Ba}_3\text{CoNb}_2\text{O}_9$ is a magnetic insulator, the measured specific heat can be expressed as a sum of magnetic and phonon terms. The high-temperature specific heat shown in the inset of Fig. 2 is attributed to the phonon specific heat. With decreasing temperature, C/T at approximately 10 K becomes almost zero, in contrast to that at lower temperatures. This indicates that the low-temperature specific heat below ~ 10 K is mostly of magnetic origin, and the phonon contribution is negligible. We thus evaluate the magnetic entropy S_{mag} of $\text{Ba}_3\text{CoNb}_2\text{O}_9$ by integrating the measured C/T with respect to T below 10 K [24]. The entropy gain is estimated to be $0.43 R \ln 2$ at T_{N1} and $0.60 R \ln 2$ at T_{N2} . With further increasing temperature, S_{mag} increases gradually and approaches approximately $R \ln 2$ at 10 K. This provides evidence that a pseudospin-1/2 description is indeed valid for $\text{Ba}_3\text{CoNb}_2\text{O}_9$ when $T < 10$ K. Below T_{N2} , the specific heat is proportional to T^3 with no residual term, which indicates the 3D spin-wave dispersions in the ordered state.

Figure 3(a) shows C/T vs T measured in several magnetic fields of up to 4 T. With

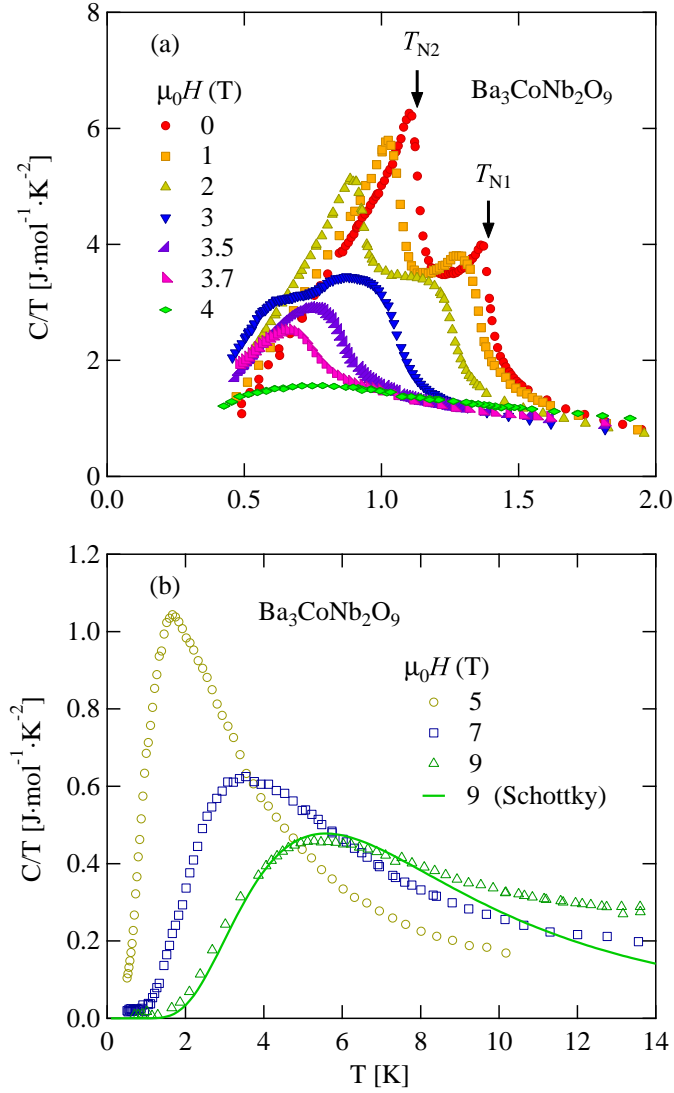


FIG. 3: (Color online) Temperature dependence of C/T in $\text{Ba}_3\text{CoNb}_2\text{O}_9$ measured in magnetic fields of (a) 0 – 4 T and (b) 5 – 9 T. The solid curve in (b) represents the Schottky contribution for the case of $H = 9$ T (see text).

increasing magnetic field, the two peaks associated with T_{N1} and T_{N2} shift to lower temperatures and become smeared. T_{N1} and T_{N2} are no more detectable for $H > 3.7$ T and $H > 3.0$ T, respectively. At a higher field of 4 T, a broad maximum can be observed around $T_{\text{max}} = 0.7$ K. As shown in Fig. 3(b), T_{max} shifts to higher temperatures with increasing field, while the peak height monotonically decreases. A solid curve is fit to the C/T data at 9 T

using the following Schottky formula:

$$C_{\text{Sch}} = Nk_B \left(\frac{g\mu_B H}{2k_B T} \right)^2 \frac{1}{\cosh^2(g\mu_B H/2k_B T)}, \quad (1)$$

where N , which is the number of atoms, and the g -factor are free parameters. Equation (1) expresses the Schottky specific heat due to the Zeeman splitting of an $S=1/2$ spin without exchange interaction between spins. The experimental data for the case of 9 T is well reproduced by eq. (1) with $g=3.0$, which is in good agreement with the results obtained from the magnetization measurements shown below. The deviation of the fitting curve from the experimental data at high temperatures is ascribed to the phonon contribution. It is also found that although T_{max} and the peak height of the Schottky anomaly vary with the applied field, the magnetic entropy S_{mag} at 10 K is close to $R \ln 2$, irrespective of the applied field. This is further evidence for the pseudospin-1/2 description of $\text{Ba}_3\text{CoNb}_2\text{O}_9$.

Figure 4(a) shows the T dependence of the magnetization divided by the field M/H in $\text{Ba}_3\text{CoNb}_2\text{O}_9$ measured at several magnetic fields of up to 4 T. The contribution of the Van Vleck paramagnetism is subtracted as will be discussed below. No thermal hysteresis is observed between the zero-field-cooled and field-cooled data. The two magnetization anomalies below 4 T, indicated by arrows for each set of data, are attributed to magnetic phase transitions. The transition temperatures T_{N1} and T_{N2} obtained at various magnetic fields are in good agreement with those obtained from specific heat measurements.

Figure 4(b) shows the raw magnetization M_{raw} in $\text{Ba}_3\text{CoNb}_2\text{O}_9$ and its field derivative as functions of H measured at 0.5 K. The highest applied field of 7 T was sufficient to reveal the entire magnetization process. The saturation field is determined to be $H_s = 4.0$ T from the inflection point of the dM_{raw}/dH curve. This small saturation field indicates that the exchange interaction in $\text{Ba}_3\text{CoNb}_2\text{O}_9$ is much smaller than that in $\text{Ba}_3\text{CoSb}_2\text{O}_9$, in which the saturation field is $H_s \simeq 32$ T [15, 16]. Above H_s , M_{raw} increases linearly with increasing field because of the large T -independent Van Vleck paramagnetism characteristic of the Co^{2+} ion in the octahedral environment [19], as observed in $\text{Ba}_3\text{CoSb}_2\text{O}_9$ [15, 16]. From the magnetization slope above H_s , we evaluate the Van Vleck paramagnetic susceptibility to be $\chi_{\text{VV}} = 6.1 \times 10^{-2} \mu_B/(\text{Co}^{2+}\text{T}) = 3.4 \times 10^{-2}$ emu/mol. By subtracting the Van Vleck term, the saturation magnetization is obtained to be $M_s = 1.5 \mu_B/\text{Co}^{2+}$, which gives an average g -factor of 3.0.

As seen from Fig. 4(b), the magnetization anomaly at H_s is considerably sharp in spite of

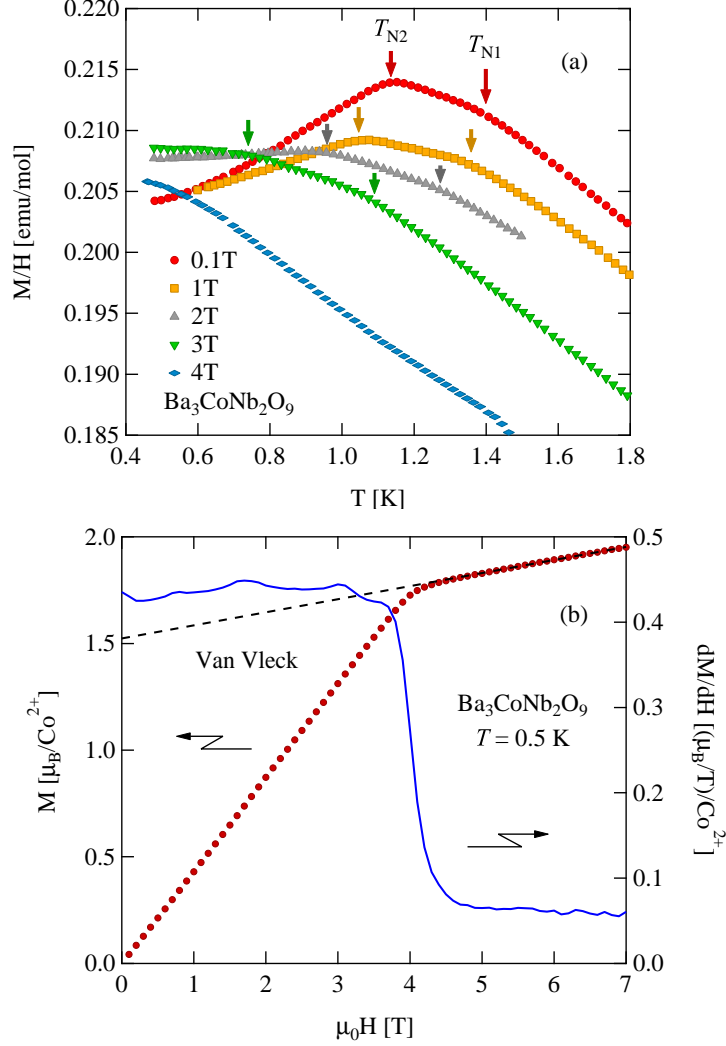


FIG. 4: (Color online) (a) Temperature dependence of magnetic susceptibility M/H in $\text{Ba}_3\text{CoNb}_2\text{O}_9$ measured at several magnetic fields of up to 4 T, where the Van Vleck paramagnetic susceptibility has been subtracted. Arrows denote the ordering temperatures T_{N1} and T_{N2} . (b) Field dependence of raw magnetization M_{raw} (left) and its field derivative dM_{raw}/dH (right) in $\text{Ba}_3\text{CoNb}_2\text{O}_9$ measured at 0.5 K. The dashed line denotes the Van Vleck paramagnetism.

powdered sample. If the g -factor and/or exchange interaction are anisotropic, the saturation field depend strongly on the field direction, so that the magnetization anomaly at H_s for powdered sample should be smeared. The sharp magnetization anomaly at H_s observed in $\text{Ba}_3\text{CoNb}_2\text{O}_9$ demonstrates that both of the g -factor and exchange interaction are nearly isotropic, as in the case for the Sb-analog compound [16].

Figure 5 shows the magnetic phase diagram of $\text{Ba}_3\text{CoNb}_2\text{O}_9$, determined via specific heat

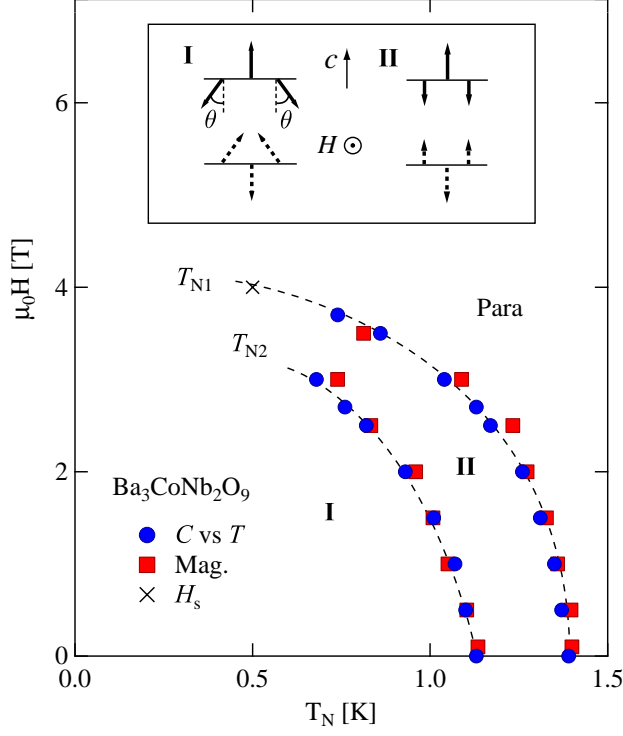


FIG. 5: (Color online) Magnetic field vs temperature phase diagram of $\text{Ba}_3\text{CoNb}_2\text{O}_9$ powder obtained from the present specific heat and magnetization measurements. Dashed curves are guides to the eyes. The spin configurations expected in the two ordered phases I and II are displayed in the inset. Solid and dashed arrows denote the spin configurations on the two neighboring triangular layers. The magnetic field is assumed to be perpendicular to the c axis.

and magnetization measurements. It has been theoretically shown that two-step magnetic ordering occurs in TLAFs when the magnetic anisotropy is of the easy-axis type, while the ordering is single-step when the anisotropy is of the easy-plane type [25, 26]. Thus, we infer that the successive phase transitions observed in $\text{Ba}_3\text{CoNb}_2\text{O}_9$ arise from easy-axis magnetic anisotropy. Note that the magnetic anisotropy in $\text{Ba}_3\text{CoSb}_2\text{O}_9$ is of the easy-plane type [16]. A small difference in the trigonal crystal field gives rise to different signs of magnetic anisotropy in these two compounds.

For the powder sample with hexagonal symmetry, the physical anomaly for the case of $H \perp c$ is more pronounced than that for $H \parallel c$ because the probability of $H \perp c$ is twice as large as that of $H \parallel c$. This was observed in the magnetization process of $\text{Ba}_3\text{CoSb}_2\text{O}_9$ powder [15, 16]. Thus, we deduce that the phase diagram shown in Fig. 5 approximates the phase diagram for $H \perp c$ in $\text{Ba}_3\text{CoNb}_2\text{O}_9$. This phase diagram is considerably different from

that for a quasi-2D TLAF with easy-axis anisotropy, as observed in $\text{Rb}_4\text{Mn}(\text{MoO}_4)_3$ [27], but similar to that for a 3D TLAF with easy-axis anisotropy, in which the antiferromagnetic interlayer exchange interaction is of the same order of magnitude as the intralayer exchange interaction, as discussed theoretically by Plumer *et al.* [28, 29]. Note that when the antiferromagnetic interlayer exchange interaction is much larger than the intralayer exchange interaction, both T_{N1} and T_{N2} increase with increasing magnetic field, as observed in CsNiCl_3 [30]. For quasi-2D TLAF with easy-axis anisotropy, the temperature range of the intermediate phase becomes narrow and vanishes with increasing magnetic field for $H \perp c$ [27]. Thus, we infer that $\text{Ba}_3\text{CoNb}_2\text{O}_9$ can be magnetically described as an antiferromagnetically stacked 3D TLAF with easy-axis anisotropy. The reason why the intralayer exchange interaction is so small as compared with that in $\text{Ba}_3\text{CoSb}_2\text{O}_9$ will be discussed later.

Possible spin configurations at each magnetic phase of $\text{Ba}_3\text{CoNb}_2\text{O}_9$ are illustrated by arrows in Fig. 5. With decreasing temperature, the c axis component of the spin becomes ordered at T_{N1} with the ferrimagnetic structure in the ab plane as $\langle S_1^z \rangle < -2\langle S_2^z \rangle = -2\langle S_3^z \rangle$. At T_{N2} , the ab plane component of the spin is ordered, such that the spins form a triangular structure in the plane including the c axis, i.e., one-third of the spins are parallel to the c axis and the remainder are canted away from the c axis. The spins on the neighboring layers are aligned antiparallel to each other because of the antiferromagnetic interlayer exchange interaction, as shown in Fig. 5. It is known that the temperature range of the intermediate phase $(T_{\text{N1}} - T_{\text{N2}})/T_{\text{N1}}$ is a measure of the magnitude of the easy-axis anisotropy relative to the intralayer exchange interaction [25, 26]. The narrow intermediate phase observed in $\text{Ba}_3\text{CoNb}_2\text{O}_9$ indicates that the easy-axis anisotropy is considerably smaller than the intralayer interaction.

In $\text{Ba}_3\text{CoSb}_2\text{O}_9$, in which the antiferromagnetic intralayer exchange interaction is much larger than the interlayer exchange interaction, the quantum $1/3$ magnetization plateau was clearly observed in both the powder [15] and single crystals [16], while no such feature was detectable in $\text{Ba}_3\text{CoNb}_2\text{O}_9$ powder samples. When the antiferromagnetic interlayer exchange interaction is comparable to the intralayer exchange interaction, the spin components perpendicular to the magnetic field form a triangular structure as shown in Fig. 5. With increasing magnetic field, the spin component parallel to the magnetic field increases and the canting angle θ decreases to become zero at a finite temperature. This leads to a transition

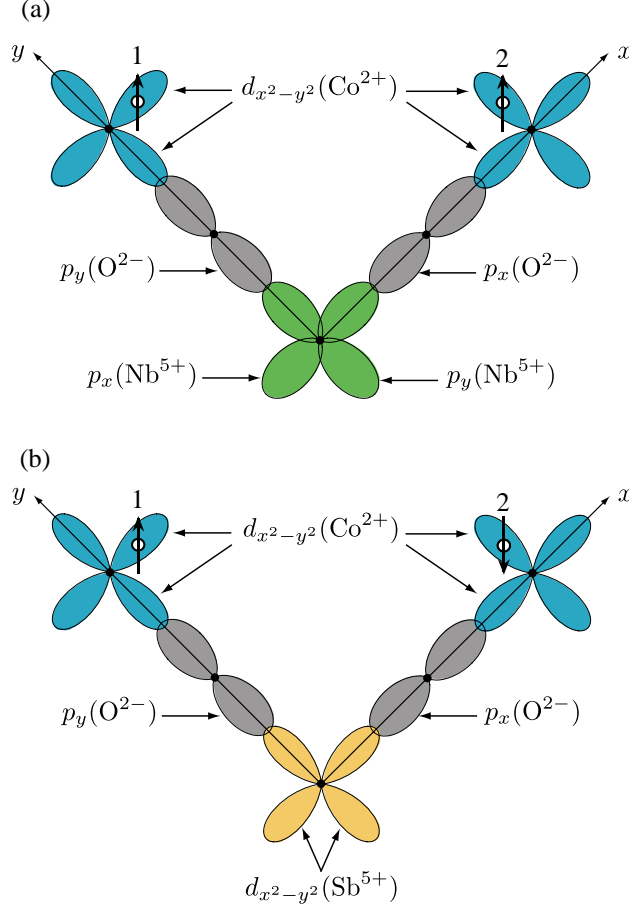


FIG. 6: (Color online) Illustrations of orbital configurations related to superexchange interactions in $\text{Ba}_3\text{CoM}_2\text{O}_9$ through $\text{Co}^{2+} - \text{O}^{2-} - M^{5+} - \text{O}^{2-} - \text{Co}^{2+}$ for (a) $M = \text{Nb}$ and (b) Sb .

from the triangular state to the collinear state [29].

Next, we discuss the reason why the antiferromagnetic intralayer exchange interaction in $\text{Ba}_3\text{CoNb}_2\text{O}_9$ is much smaller than that in $\text{Ba}_3\text{CoSb}_2\text{O}_9$, on the basis of the Kanamori theory.[31] In Ref.31, it has been theoretically shown that, when the magnetic cation is subjected to the octahedral crystalline field, the sign of the superexchange interaction via nonmagnetic anion is closely connected with the orbital states of cation and anion. Kanamori theory is useful to discuss qualitatively whether the superexchange interaction is ferromagnetic or antiferromagnetic. In $\text{Ba}_3\text{CoNb}_2\text{O}_9$ and $\text{Ba}_3\text{CoSb}_2\text{O}_9$, Co^{2+} spins in the same layer interact via superexchange interactions through $\text{Co}^{2+} - \text{O}^{2-} - \text{O}^{2-} - \text{Co}^{2+}$ and $\text{Co}^{2+} - \text{O}^{2-} - M^{5+} - \text{O}^{2-} - \text{Co}^{2+}$ paths with $M = \text{Nb}, \text{Sb}$. The superexchange interaction through $\text{Co}^{2+} - \text{O}^{2-} - \text{O}^{2-} - \text{Co}^{2+}$ is common to both systems and should be antiferromagnetic as observed in many magnetic compounds. Thus, it is considered that the difference in

the exchange interaction between these two systems arises from the filled outermost orbitals, which are $4p$ and $4d$ orbitals for $\text{Ba}_3\text{CoNb}_2\text{O}_9$ and $\text{Ba}_3\text{CoSb}_2\text{O}_9$, respectively. We consider the superexchange interaction between hole spins on the $d_{x^2-y^2}$ orbitals of Co^{2+} ions. The possible exchange paths are illustrated in Fig. 6. Here, we assume for simplification that successive Co^{2+} , O^{2-} and M^{5+} ions are on a straight line and the bond angle of $\text{O}^{2-} - \text{M}^{5+} - \text{O}^{2-}$ is 90° . The superexchange mechanism for $M = \text{Nb}$ is based on the following perturbation process: (1) Hole 1 with up spin on the left Co^{2+} is first transferred to the p_y orbital of O^{2-} , which is combined with the p_y orbital of Nb^{5+} to form a molecular orbital. (2) Hole 2 on the right Co^{2+} is also transferred to the other molecular orbital composed of two p_x orbitals of O^{2-} and Nb^{5+} . In this case, the total energy of the system is decreased when the spin of hole 2 is up, because in the Nb^{5+} ion, the two hole spins on the p_y and p_x orbitals have to be parallel owing to the Hund rule. (3) The two holes are transferred back to the $d_{x^2-y^2}$ orbitals of Co^{2+} . Consequently, a ferromagnetic superexchange interaction takes place. On the other hand, the superexchange for $M = \text{Sb}$ should be antiferromagnetic because in the Sb^{5+} ion, the two hole spins on the same $d_{x^2-y^2}$ have to be antiparallel to each other owing to the Pauli principle. Similar results are also obtained for the hole spins on the $d_{3z^2-r^2}$ orbitals of Co^{2+} ions. We infer that for $M = \text{Nb}$, antiferromagnetic and ferromagnetic superexchange interactions through $\text{Co}^{2+} - \text{O}^{2-} - \text{O}^{2-} - \text{Co}^{2+}$ and $\text{Co}^{2+} - \text{O}^{2-} - \text{M}^{5+} - \text{O}^{2-} - \text{Co}^{2+}$, respectively, mostly cancel out, so that the resultant antiferromagnetic exchange interaction becomes small. However, for $M = \text{Sb}$, the superexchange interactions through these two paths are both antiferromagnetic, and the total antiferromagnetic exchange interaction is enhanced. For this reason, the antiferromagnetic intralayer exchange interaction in $\text{Ba}_3\text{CoNb}_2\text{O}_9$ could be much smaller than that in $\text{Ba}_3\text{CoSb}_2\text{O}_9$. In order to determine the detailed magnetic parameters, further experimental and theoretical approaches such as a neutron scattering measurement and density-functional calculations are needed.

IV. CONCLUSION

In summary, we have performed low-temperature specific heat and magnetization measurements on $\text{Ba}_3\text{CoNb}_2\text{O}_9$ powder. $\text{Ba}_3\text{CoNb}_2\text{O}_9$ exhibits two magnetic transitions at $T_{\text{N1}} = 1.39$ K and $T_{\text{N2}} = 1.13$ K with a narrow intermediate phase, which arise from the weak easy-axis magnetic anisotropy. The magnetization saturates at $H_s = 4.0$ T. This small

saturation field shows that the intralayer exchange interaction is much smaller than that in $\text{Ba}_3\text{CoSb}_2\text{O}_9$. The difference in the filled outermost orbitals of Nb^{5+} and Sb^{5+} gives rise to considerably different exchange interactions in both systems. The magnetic field vs temperature phase diagram shown in Fig. 5, which is considered to approximate that for $H \perp c$, is in accordance with that for a TLAF with a strong interlayer exchange interaction and small easy-axis anisotropy [28, 29]. Therefore, $\text{Ba}_3\text{CoNb}_2\text{O}_9$ can be described as an $S = 1/2$ antiferromagnetically stacked 3D TLAF with easy-axis anisotropy, in contrast to quasi-2D $\text{Ba}_3\text{CoSb}_2\text{O}_9$ [15, 16]. Note that our conclusion is different from the conclusion by Lee *et al.* [32], although most of our experimental results are consistent with theirs. They attributed the field-induced phase transitions observed in $\text{Ba}_3\text{CoNb}_2\text{O}_9$ to quantum fluctuations characteristic of quasi-2D TLAF. $\text{Ba}_3\text{CoNb}_2\text{O}_9$ could be a useful model for obtaining a comprehensive understanding of the $S = 1/2$ TLAFs.

ACKNOWLEDGMENTS

This work was supported by a Grant-in-Aid for Scientific Research (A) from the Japan Society for the Promotion of Science, and the Global COE Program “Nanoscience and Quantum Physics” at Tokyo Tech. funded by the Ministry of Education, Culture, Sports, Science and Technology of Japan.

-
- [1] P. Anderson, Mater. Res. Bull. **8**, 153 (1973).
 - [2] M. Mekata, J. Phys. Soc. Jpn. **42**, 76 (1977).
 - [3] M. F. Collins and O. A. Petrenko, Can. J. Phys. **75**, 605 (1997).
 - [4] H. Kawamura, J. Phys.: Condens. Matter **10**, 4707 (1998).
 - [5] L. Balents, Nature **464**, 199 (2010).
 - [6] J. Villian, R. Bidaux, J. P. Carton, and R. J. Conte, J. Phys. (Paris) **41**, 1263 (1980).
 - [7] H. Nishimori and S. Miyashita, J. Phys. Soc. Jpn. **55**, 4448 (1986).
 - [8] A. V. Chubokov and D. I. Golosov, J. Phys. Condens. Matter **3**, 69 (1991).
 - [9] D. J. J. Farnell, R. Zinke, J. Schulenburg, and J. Richter, J. Phys.: Condens. Matter **21**, 406002 (2009).

- [10] A. Honecker, J. Phys.: Condens. Matter **11**, 4697 (1999).
- [11] T. Sakai and H. Nakano, Phys. Rev. **B 83**, 100405(R) (2011).
- [12] C. Hotta, S. Nishimoto, and N. Shibata, Phys. Rev. **B 87**, 115128 (2013).
- [13] T. Ono, H. Tanaka, H. Aruga Katori, F. Ishikawa, H. Mitamura, and T. Goto, Phys. Rev. **B 67**, 104431 (2003).
- [14] N. A. Fortune, S. T. Hannahs, Y. Yoshida, T. E. Sherline, T. Ono, H. Tanaka, and Y. Takano, Phys. Rev. Lett. **102**, 257201 (2009).
- [15] Y. Shirata, H. Tanaka, A. Matsuo, and K. Kindo, Phys. Rev. Lett. **108**, 057205 (2012).
- [16] T. Susuki, N. Kurita, T. Tanaka, H. Nojiri, A. Matsuo, K. Kindo, and H. Tanaka, Phys. Rev. Lett. **110**, 267201 (2013).
- [17] A. Abragam and M. H. L. Pryce, Proc. R. Soc. (London) A **206**, 173 (1956).
- [18] M. E. Lines, Phys. Rev. **131**, 546 (1963).
- [19] T. Oguchi, J. Phys. Soc. Jpn. **20**, 2236 (1965).
- [20] U. Treiber and S. Kemmler-Sack, Z. Anorg. Allg. Chem. **487**, 161 (1982).
- [21] V. Ting, Y. Liu, L. Norén, R. L. Withers, D. J. Goossens, M. James, C. Ferraris, J. Solid State Chem. **177**, 4428 (2004).
- [22] V. Ting, Y. Liu, R. L. Withers, and L. Norén, J. Solid State Chem. **177**, 2295 (2004).
- [23] Y. Doi, Y. Hinatsu, and K. Ohoyama, J. Phys.: Condens. Matter **16**, 8923 (2004).
- [24] The temperature dependence of S_{mag} for $T \leq 0.4$ K is deduced from a smooth extrapolation using the higher temperature C/T data.
- [25] F. Matsubara, J. Phys. Soc. Jpn. **51**, 2424 (1982).
- [26] S. Miyashita and H. Kawamura, J. Phys. Soc. Jpn. **54**, 3385 (1985).
- [27] R. Ishii, S. Tanaka, K. Onuma, Y. Nambu, M. Tokunaga, T. Sakakibara, N. Kawashima, Y. Maeno, C. Broholm, D. P. Gautreaux, J. Y. Chan, and S. Nakatsuji: Eur. Phys. Lett. **94**, 17001 (2011).
- [28] M. L. Plumer, K. Hood, and A. Caille, Phys. Rev. Lett. **60**, 45 (1988).
- [29] M. L. Plumer, A. Caille, and K. Hood, Phys. Rev. **B 39**, 4489 (1989).
- [30] P. B. Johnson, J. A. Rayne, and S. A. Friedberg, J. Appl. Phys. **50**, 1853 (1979).
- [31] J. Kanamori, J. Phys. Chem. Solids **10**, 87 (1959).
- [32] M. Lee, J. Hwang, E. S. Choi, J. Ma, C. R. Dela Cruz, M. Zhu, X. Ke, Z. L. Dun, and H. D. Zhou, Phys. Rev. **B 89**, 104420 (2014).